A fast inverse kinematic solution for the nonlinear actuating mechanisms of a small-scale helicopter

Sepehr P. Khaligh, Farbod Fahimi & Charles Robert Koch

Multibody System Dynamics

ISSN 1384-5640

Multibody Syst Dyn
DOI 10.1007/s11044-015-9452-0

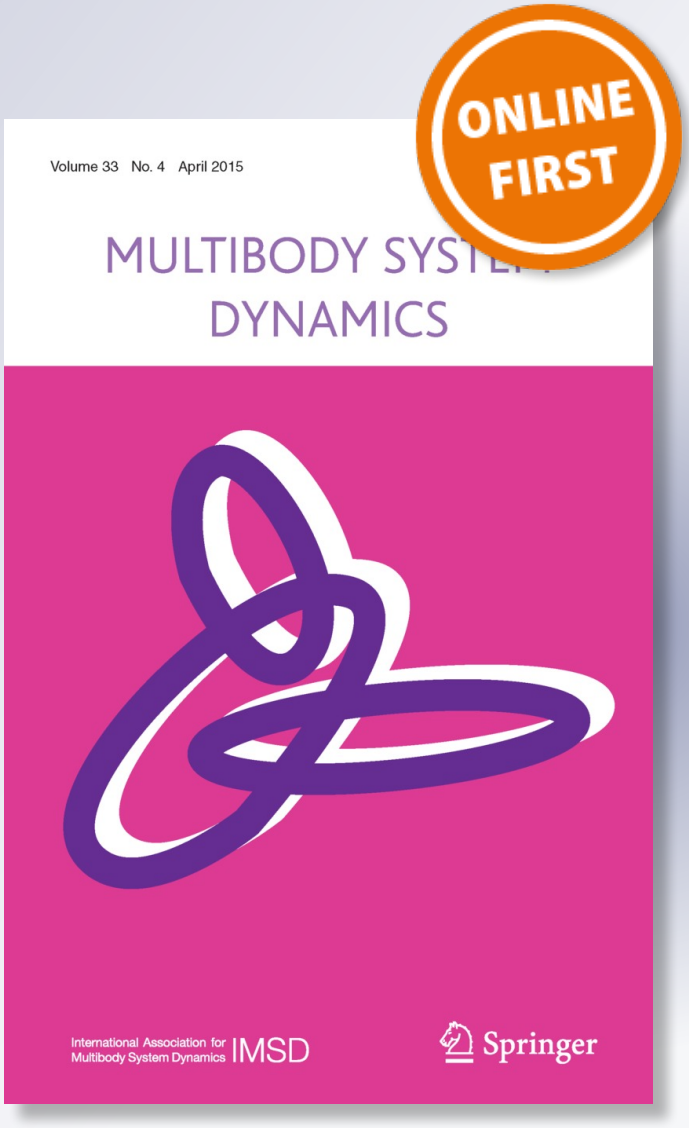

Springer

Multibody Syst Dyn
DOI 10.1007/s11044-015-9452-0

A fast inverse kinematic solution for the nonlinear actuating mechanisms of a small-scale helicopter

Sepehr P. Khaligh[1] · Farbod Fahimi[2] · Charles Robert Koch[1]

Received: 1 March 2014 / Accepted: 3 March 2015

Abstract An inverse kinematic solution for the main rotor actuating mechanism of a small-scale helicopter that includes a four-point swashplate system and a Bell–Hiller mixer and the tail rotor actuating mechanism are derived using an approach that is suitable for real-time control applications. A closed-form solution is obtained for the inverse kinematics of the swashplate mechanism and for the forward and inverse kinematics of the tail rotor. Then, a computationally efficient solution is obtained for the inverse kinematics of the Bell–Hiller mixer by converting the nonlinear kinematic equations into a generalized eigenvalue problem. The nonlinear kinematic model is compared to a linear approximation and is validated using experiments.

Keywords Actuating mechanisms · Inverse kinematics · Small-scale helicopters · Swashplate mechanism · Bell–Hiller mixer · Tail rotor mechanism

1 Introduction

The core actuating mechanism of the main rotor of a small-scale unmanned helicopter, often referred to as the Bell–Hiller mixer, is a multibody system composed of spatial linkage mechanisms which are complex and nonlinear and therefore, difficult to mathematically model without linearizing and simplifying. An accurate and fast solution for the inverse kinematics of the actuating mechanisms of a helicopter is essential for calculating the required servo inputs for real-time control applications. An accurate kinematic model, also provides a useful tool for improving the design of the helicopter's actuating mechanisms and for evaluating the performance of the fly-by-wire actuation systems [1].

To design a model-based controller for a small-scale helicopter, a kinematic model of the swashplate and Bell–Hiller mixer is required. A kinematic model of a 3-point swashplate

✉ S. P. Khaligh
sepehr.khaligh@ualberta.ca

[1] Department of Mechanical Engineering, University of Alberta, Edmonton, AB, Canada

[2] Department of Mechanical and Aerospace Engineering, University of Alabama in Huntsville, Huntsville, AL, USA

Published online: 27 March 2015

mechanism and Bell–Hiller mixer of an IKarus ECO small-scale helicopter is presented in [2]. This linear model is obtained using the small angle assumptions. Another approach for the kinematic modeling of a small-scale helicopter is described in [3], where experimental data from the actuating mechanism is collected and a curve-fitting method is used to obtain a linear relation between the servo inputs and the pitch angle of the main and tail rotor blades. Linear models do not accurately represent the kinematics of the helicopter's actuating mechanism for the entire range of the servos.

System identification is another approach used to identify the kinematics of the helicopter's actuating mechanism [4, 5]. A linear kinematic model is assumed as the actuating mechanism of a small-scale helicopter and coefficients are defined to incorporate the kinematics into the transfer function of the helicopter dynamics around certain operating points. Then, system identification in the frequency-domain is used to estimate these coefficients and unknown parameters of the system dynamics. These identified coefficients depend on the particular operating point such as the hover and cruise flight and are not adequate for nonlinear control of the helicopter in a wide range of flight regimes.

Nonlinear approaches are also used to obtain the inverse kinematics of the helicopter's actuating mechanisms. A nonlinear approach for the main rotor actuating mechanism of a small-scale helicopter is presented in [9]. The Bell–Hiller mixer is modeled by deriving the loop-closure equations in the Cartesian coordinates and then using the dialytic elimination method [12]. This results in 48 solutions when solving a 48th-order polynomial and requires applying a large number of additional constraints to find the true solution. This method is too complex for real-time control applications.

A kinematic analysis of a swashplate mechanism used in a CL-327 Guardian unmanned aerial vehicle (UAV) is presented in [10]. This UAV has two co-axial counter rotating rotors with six blades (2.03 m long) and a 100 kg payload capacity. A combination of a 3-point swashplate system and a Bell mechanism is used to change the blade angles and control the altitude and attitude of the UAV. A parallel manipulator approach is used to obtain the nonlinear direct and inverse kinematics of the swashplate and Bell mechanisms [13]. Then, a contour method is used to solve the nonlinear kinematic equations resulting in 36 solutions, which is again not suitable for real-time control applications [14].

Another kinematic model for a 3-point swashplate mechanism and the Bell–Hiller mixer of a small-scale helicopter is described in [11]. A set of nonlinear algebraic equations must be solved using iterative numerical methods which requires a high amount of computations and is not suitable for real-time control applications.

Kinematic approaches that are based on the linearized model of the helicopter's actuating mechanisms [2–8] are not accurate for the entire range of the servo actuators. Typically, nonlinear kinematic approaches result in a large number of solutions requiring many computations [9–11] which are not suitable for real-time control applications. Moreover, kinematics of a 3-point swashplate mechanism is widely discussed in the literature, while a kinematic analysis of a four-point swashplate mechanism, used in many small-scale helicopters, is still lacking in the literature.

In this work, a detailed nonlinear inverse kinematics of the main rotor actuating mechanism including a four-point swashplate mechanism and the Bell–Hiller mixer as well as the actuating mechanism of the tail rotor are derived for a small-scale helicopter using the vector loops approach in the Isotropic coordinates. Then, a fast solution is obtained for the inverse kinematics of the Bell–Hiller mixer by converting the nonlinear equations into a generalized eigenvalue problem using the Sylvester-Type Elimination method [15]. Then, the nonlinear kinematic model is compared to a linear approximation of the system kinematics and is validated with experiments. The main contributions of this paper are:

(a) The complex closed-form nonlinear inverse kinematic analysis of the Bell–Hiller mechanism with a four-point swashplate is systematically broken down for easy use by helicopter mechanism designers and control engineers alike.
(b) The closed-form nonlinear kinematic model has been successfully correlated with experimental results.
(c) This theoretical/experimental technique is applicable to similar mechanisms, allowing designers to use the nonlinear model to find the exact range of linear operation of their Bell–Hiller mixer.
(d) This approach provides a fast and accurate solution for the inverse kinematics of the helicopter's main and tail rotor actuating mechanisms allowing for the required servo inputs to be calculated in real-time as in [16, 17].
(e) Design improvements of the helicopter's actuating mechanisms and performance evaluation of fly-by-wire actuation systems can also be examined.

The remainder of this paper is organized into sections. In Sect. 2, the inverse kinematics of the main rotor including the swashplate and the Bell–Hiller mixer is described. Next, the tail rotor mechanism is described in Sect. 3. The experimental validation of the kinematic model is presented in Sect. 4 and conclusions are presented in the last section.

2 Main rotor mechanism

The main rotor actuating mechanism of a small-scale helicopter is composed of two complex linkage mechanisms: the swashplate mechanism and the Bell–Hiller mixer. First, the kinematic equations of a four-point swashplate mechanism used in a small scale helicopter are derived. Then, the kinematic model of the Bell–Hiller mixer is derived in the next section.

2.1 Swashplate mechanism

A minimum of three servos is required to control the three-dimensional motion of the swashplate. In a three-point swashplate, three servos are connected to the swashplate in a 120° arrangement while in a four-point swashplate a 90° arrangement is used. As shown in the swashplate mechanism in Fig. 1, all four servos have to move up and down together in a four-point swashplate system to control the collective pitch of the blades, while only two opposing servos have to move in opposite directions to control the pure longitudinal or lateral cyclic pitch of the blades. For example, in a forward flight maneuver, servo 1 lowers the arm j1b1 and servo 3 raises the arm j3b3 and servos 2 and 4 remain at their positions to tilt the swashplate forward without having a vertical displacement. This position of the swashplate causes the main rotor disk to tilt forward as required in a forward flight maneuver. Therefore, a four-point swashplate mechanism has the advantage of requiring less torques from the servos during all maneuvers due to having an extra servo.

The swashplate mechanism, shown in Fig. 1, is composed of two pinned plates, one rotating and the other one stationery. Four servos allow for a three-dimensional motion of the lower stationery plate which cause certain points on the upper rotating plate such as A and B to experience different movements as the azimuth angle changes.

The motion of the swashplate is characterized by two successive Euler rotations, δ_x and δ_y, respectively around x_1 and y_1 axes of the fixed coordinates $\{x_1 y_1 z_1\}$ attached to the swashplate's lower stationery plate at the point C and the vertical displacement z_c from the center of the swashplate, point C, to the origin of the reference coordinate $\{x_i y_i z_i\}$, point O.

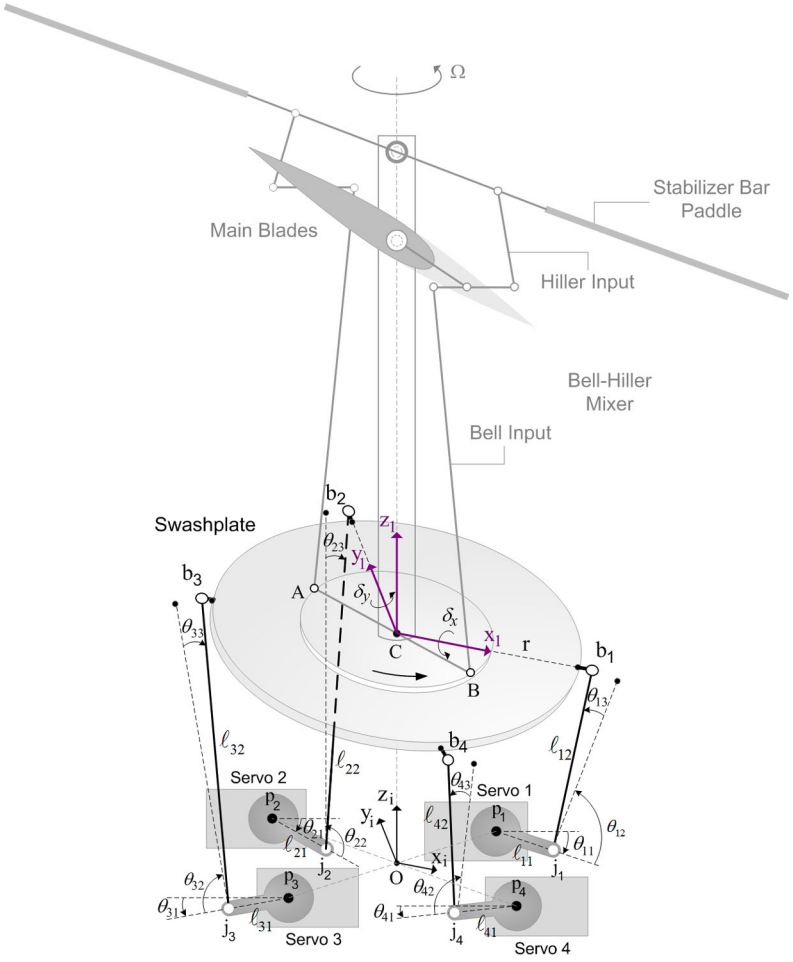

Fig. 1 Helicopter Swashplate mechanism

The forward kinematics of the swashplate is used to calculate the swashplate's orientations δ_x and δ_y, and displacement z_c, in terms of the corresponding servo angles θ_{11} to θ_{41}.

To derive the forward and inverse kinematics of the swashplate mechanism, the method used in [11] is extended to a four-point swashplate mechanism. In this method, the position of each corner point b_1 to b_4, is calculated using two different kinematic loops. Then the kinematic equations are derived by equating the relations found from each kinematic loop. For instance, the position of the point b_1 can be calculated either through the linkage $Op_1j_1b_1$ expressed in the reference coordinates $\{x_i\, y_i\, z_i\}$, or by expressing its position first in the local coordinates $\{x_1\, y_1\, z_1\}$ and then in the reference coordinates $\{x_i\, y_i\, z_i\}$ through a homogeneous transformation. This procedure is repeated for all four points on the swashplate as

$$\mathbf{R}^i_{bj} = \mathbf{H}^i_1 r_{b_j} = \mathbf{T}_{y,y_{p_j}} \mathbf{T}_{x,x_{p_j}} \mathbf{R}_{y,\theta_{j1}} \mathbf{T}_{x,\ell_{j1}} \mathbf{R}_{y,\theta_{j2}} \mathbf{R}_{z,\theta_{j3}} \mathbf{l}_{b_j}, \quad j = 1, \ldots, 4, \tag{1}$$

where

$$\mathbf{r}_{b_1} = [\,r \quad 0 \quad 0 \quad 1\,]^T, \qquad \mathbf{r}_{b_2} = [\,0 \quad r \quad 0 \quad 1\,]^T, \qquad \mathbf{r}_{b_3} = [\,-r \quad 0 \quad 0 \quad 1\,]^T,$$
$$\mathbf{r}_{b_4} = [\,0 \quad -r \quad 0 \quad 1\,]^T, \qquad \mathbf{l}_{b_1} = [\,\ell_{12} \quad 0 \quad 0 \quad 1\,]^T, \qquad \mathbf{l}_{b_2} = [\,\ell_{22} \quad 0 \quad 0 \quad 1\,]^T,$$
$$\mathbf{l}_{b_3} = [\,-\ell_{32} \quad 0 \quad 0 \quad 1\,]^T, \qquad \mathbf{l}_{b_4} = [\,-\ell_{42} \quad 0 \quad 0 \quad 1\,]^T,$$

$\mathbf{H}_1^i$ is the homogeneous transformation between the coordinates $\{x_1 y_1 z_1\}$ and $\{x_i y_i z_i\}$ defined as

$$\mathbf{H}_1^i = \mathbf{T}_{z,z_c}\mathbf{R}_{y,\delta_y}\mathbf{R}_{x,\delta_x}, \tag{2}$$

and $\mathbf{R}$ and $\mathbf{T}$ are homogenous rotation and transformation matrices defined as

$$\mathbf{R}_{x,\delta_x} = \begin{bmatrix} 1 & 0 & 0 & 0 \\ 0 & \cos\delta_x & -\sin\delta_x & 0 \\ 0 & \sin\delta_x & \cos\delta_x & 0 \\ 0 & 0 & 0 & 1 \end{bmatrix}, \qquad \mathbf{R}_{y,\delta_y} = \begin{bmatrix} \cos\delta_y & 0 & \sin\delta_y & 0 \\ 0 & 1 & 0 & 0 \\ -\sin\delta_y & 0 & \cos\delta_y & 0 \\ 0 & 0 & 0 & 1 \end{bmatrix},$$
$$\mathbf{T}_{x,\ell_{11}} = \begin{bmatrix} 1 & 0 & 0 & \ell_{11} \\ 0 & 1 & 0 & 0 \\ 0 & 0 & 1 & 0 \\ 0 & 0 & 0 & 1 \end{bmatrix}, \qquad \mathbf{T}_{y,y_{p_1}} = \begin{bmatrix} 1 & 0 & 0 & 0 \\ 0 & 1 & 0 & y_{p_1} \\ 0 & 0 & 1 & 0 \\ 0 & 0 & 0 & 1 \end{bmatrix}, \tag{3}$$
$$\mathbf{T}_{z,z_c} = \begin{bmatrix} 1 & 0 & 0 & 0 \\ 0 & 1 & 0 & 0 \\ 0 & 0 & 1 & z_c \\ 0 & 0 & 0 & 1 \end{bmatrix}.$$

Expanding Eq. (1) results in:

$$\begin{aligned}
&r\cos\delta_y - x_{p_1} = \ell_{12}\cos(\theta_{11}+\theta_{12})\cos\theta_{13} + \ell_{11}\cos\theta_{11},\\
&r\sin\delta_y - z_c = \ell_{12}\sin(\theta_{11}+\theta_{12})\cos\theta_{13} + \ell_{11}\sin\theta_{11},\\
&\cos^2\theta_{13} = 1 - \left(\frac{y_{p_1}}{\ell_{12}}\right)^2,\\
&r\sin\delta_x\sin\delta_y - x_{p_2} = \ell_{22}\cos(\theta_{21}+\theta_{22})\cos\theta_{23} + \ell_{21}\cos\theta_{21},\\
&-r\sin\delta_x\cos\delta_y - z_c = \ell_{22}\sin(\theta_{21}+\theta_{22})\cos\theta_{23} + \ell_{21}\sin\theta_{21},\\
&\cos^2\theta_{23} = 1 - \left(\frac{r\cos\delta_x - y_{p_2}}{\ell_{22}}\right)^2,\\
&r\cos\delta_y + x_{p_3} = \ell_{32}\cos(\theta_{31}+\theta_{32})\cos\theta_{33} + \ell_{31}\cos\theta_{31},\\
&r\sin\delta_y + z_c = \ell_{32}\sin(\theta_{31}+\theta_{32})\cos\theta_{33} + \ell_{31}\sin\theta_{31},\\
&\cos^2\theta_{33} = 1 - \left(\frac{y_{p_3}}{\ell_{32}}\right)^2,\\
&r\sin\delta_x\sin\delta_y + x_{p_4} = \ell_{42}\cos(\theta_{41}+\theta_{42})\cos\theta_{43} + \ell_{41}\cos\theta_{41},\\
&-r\sin\delta_x\cos\delta_y + z_c = \ell_{42}\sin(\theta_{41}+\theta_{42})\cos\theta_{43} + \ell_{41}\sin\theta_{41},\\
&\cos^2\theta_{43} = 1 - \left(\frac{r\cos\delta_x + y_{p_4}}{\ell_{42}}\right)^2.
\end{aligned} \tag{4}$$

The left-hand side terms of Eq. (4) are denoted by n_i, $i = 1, \ldots, 12$. The first, second, fourth, fifth, seventh, eighth, tenth, and eleventh terms in Eq. (4) are rearranged, then squared to obtain:

$$\begin{aligned}
(n_1 - \ell_{11}\cos\theta_{11})^2 &= \ell_{12}^2 \cos^2(\theta_{11} + \theta_{12})\cos^2\theta_{13},\\
(n_2 - \ell_{11}\sin\theta_{11})^2 &= \ell_{12}^2 \sin^2(\theta_{11} + \theta_{12})\cos^2\theta_{13},\\
(n_4 - \ell_{21}\cos\theta_{21})^2 &= \ell_{22}^2 \cos^2(\theta_{21} + \theta_{22})\cos^2\theta_{23},\\
(n_5 - \ell_{21}\sin\theta_{21})^2 &= \ell_{22}^2 \sin^2(\theta_{21} + \theta_{22})\cos^2\theta_{23},\\
(n_7 - \ell_{31}\cos\theta_{31})^2 &= \ell_{32}^2 \cos^2(\theta_{31} + \theta_{32})\cos^2\theta_{33},\\
(n_8 - \ell_{31}\sin\theta_{31})^2 &= \ell_{32}^2 \sin^2(\theta_{31} + \theta_{32})\cos^2\theta_{33},\\
(n_{10} - \ell_{41}\cos\theta_{41})^2 &= \ell_{42}^2 \cos^2(\theta_{41} + \theta_{42})\cos^2\theta_{43},\\
(n_{11} - \ell_{41}\sin\theta_{41})^2 &= \ell_{42}^2 \sin^2(\theta_{41} + \theta_{42})\cos^2\theta_{43}.
\end{aligned} \tag{5}$$

The third, sixth, ninth, and twelfth equations in Eq. (4) indicate that $n_3 = \cos^2\theta_{13}$, $n_6 = \cos^2\theta_{23}$, $n_9 = \cos^2\theta_{33}$, $n_{12} = \cos^2\theta_{43}$. Substituting these into Eq. (5), and summing up the squares of relevant pairs of equations in Eq. (5) yields:

$$(n_1 - \ell_{11}\cos\theta_{11})^2 + (n_2 - \ell_{11}\sin\theta_{11})^2 = n_3\ell_{12}^2, \tag{6}$$

$$(n_4 - \ell_{21}\cos\theta_{21})^2 + (n_5 - \ell_{21}\sin\theta_{21})^2 = n_6\ell_{22}^2, \tag{7}$$

$$(n_7 - \ell_{31}\cos\theta_{31})^2 + (n_8 - \ell_{31}\sin\theta_{31})^2 = n_9\ell_{32}^2, \tag{8}$$

$$(n_{10} - \ell_{41}\cos\theta_{41})^2 + (n_{11} - \ell_{41}\sin\theta_{41})^2 = n_{12}\ell_{42}^2. \tag{9}$$

Given the values of the servo inputs, the unknown variables of the swashplate mechanism, δ_x, δ_y and z_c can be calculated using Eqs. (6)–(9). This set of nonlinear algebraic equations does not have a closed-form solution and must be solved using numerical methods. One possible solution method is to first solve Eqs. (6) and (8) for δ_y and z_c and then solve Eq. (7) for δ_x. Next, the calculated unknown variables, δ_x, δ_y and z_c, are checked to satisfy Eq. (9). However, for the inverse kinematic of the swashplate mechanism a closed-form analytical solution is required for the control design and is described next.

To derive the inverse kinematics of the swashplate, Eqs. (6)–(9) are used to calculate the servo angles, θ_{11} to θ_{41}, in terms of the swashplate's orientations δ_x and δ_y, and displacement z_c. By expanding and rearranging Eqs. (6)–(9), the inverse kinematic of the swashplate mechanism is calculated as:

$$\theta_{j1} = \arccos\left(\frac{\ell_{j1}^2 - n_{3j}\ell_{j2}^2 + n_{3j-2}^2 + n_{3j-1}^2}{2n_{3j-2}\ell_{j1}}\cos\beta_j\right) + \beta_j, \quad j = 1, \ldots, 4, \tag{10}$$

where

$$\beta_j = \arctan\left(\frac{n_{3j-1}}{n_{3j-2}}\right), \quad j = 1, \ldots, 4. \tag{11}$$

2.2 Bell–Hiller mixer

The pitch angle of the main rotor blades can be changed both collectively and cyclically. The Bell–Hiller mixer is the core part of the main rotor actuating mechanism allowing changes in both the collective and cyclic pitch angles of the main rotor blades by mixing the Bell and Hiller inputs as shown in Fig. 2. The pitch angle of the main rotor blades can be represented

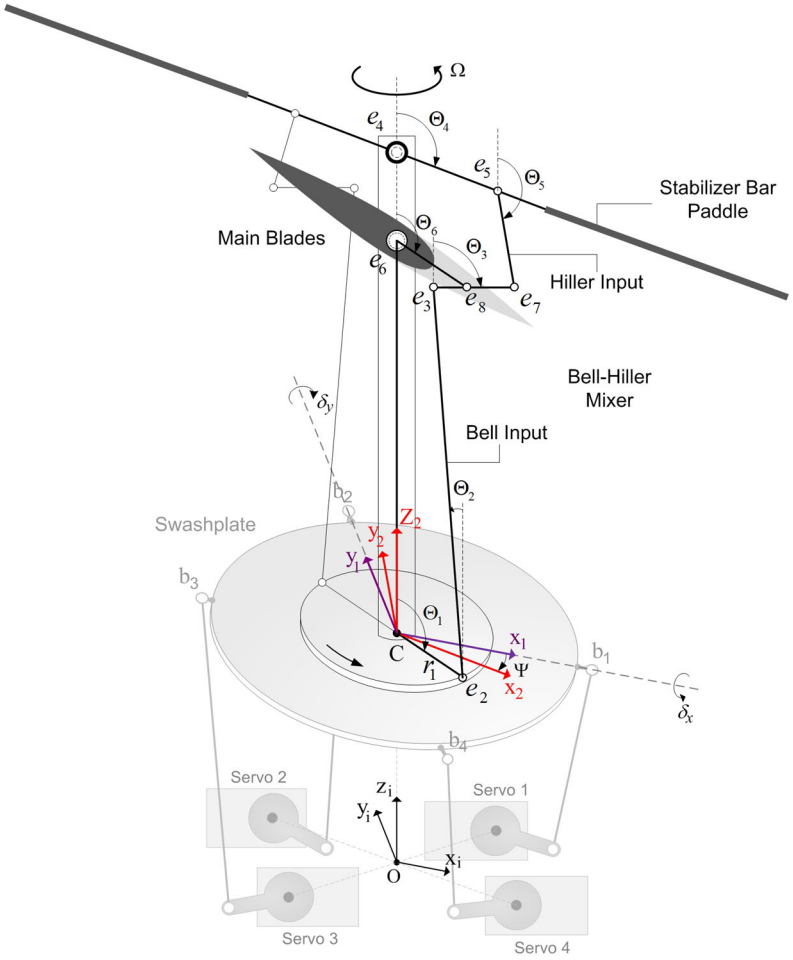

Fig. 2 Helicopter Bell–Hiller mixer

by the first harmonic components of the Fourier series expansion in terms of the azimuth angle Ψ

$$\theta_{\text{mr}} = \delta_{\text{col}} + \delta_{\text{lat}} \sin(\Psi) + \delta_{\text{lon}} \cos(\Psi). \tag{12}$$

Solving the inverse kinematics of the Bell–Hiller mixer results in the corresponding orientations δ_x and δ_y, and displacement z_c, of the swashplate in terms of the desired collective and cyclic pitch of the blades. This is a complicated 12-bar linkage mechanism, as shown in Fig. 2, with inputs as the pitch angle of the main blade Θ_6, and the flapping angle of the stabilizer bar Θ_4, and the outputs as the swashplate orientations δ_x and δ_y, and the displacement z_c. The kinematic equations of the Bell–Hiller mixer are derived in two steps below.

Table 1 Parameters of the Bell–Hiller mixer

$a_0 = \ell_{e_6e_4}$	$a_3 = \ell_{e_3e_8}$	$a_6 = \ell_{e_6e_8}$
$a_1 = \ell_{Ce_2}$	$a_4 = \ell_{e_4e_5}$	$b_1 = \ell_{e_8e_7}$
$a_2 = \ell_{e_2e_3}$	$a_5 = \ell_{e_5e_7}$	$S = \ell_{Ce_6}$

2.3 Collective pitch to swashplate displacement

First, the inverse kinematics of the Bell–Hiller mixer is derived so that the vertical displacement of the swashplate z_c is obtained in terms of the collective pitch of the main rotor δ_{col}. To do this, the kinematic equations are derived for the azimuth angle at zero cyclic pitch where the blades only have a collective pitch. In the second step, the kinematic equations are derived so that the orientations of the swashplate δ_x and δ_y, are obtained in terms of the cyclic pitch of the main rotor.

The inverse kinematics of the Bell–Hiller mixer does not have a closed-form solution. Therefore, a fast numerical approach is developed in this section to solve the inverse kinematics of the Bell–Hiller mixer. To do this, the kinematic equations of the Bell–Hiller mixer are derived in the Isotropic coordinates using the "vector loops" approach to minimize the computations.

Since the Bell–Hiller mixer is a symmetrical mechanism, a seven-bar linkage (a half-model of the mechanism shown in Fig. 2) is used for simplicity. To obtain the inverse kinematics of this linkage, the kinematic equations for the loop-closures "C2386C" and "457864" are derived. First, the following variables are defined:

$$\theta_i = e^{i\Theta_i} = \cos\Theta_i + i\sin\Theta_i, \quad i = 1, \ldots, 6, \tag{13}$$

where Θ_i are the linkage angles shown in Fig. 2 in radians. For example, the angle Θ_6 is the input to the inverse kinematics and is related to the collective pitch as

$$\Theta_6 = \frac{\pi}{2} - \delta_{\text{col}}. \tag{14}$$

The length variables a_i and b_i are defined in Table 1. Since the kinematic equations relating the vertical displacement of the swashplate to the collective pitch of the blade is desired in this step, the variables $\theta_1, \theta_4, \theta_6$ are defined as the inputs, and $\theta_2, \theta_3, \theta_5$ and S are defined as the outputs of the mechanism. Modeling the links as vectors in the complex plane results in:

$$\begin{aligned} S + a_6\theta_6 &= a_1\theta_1 + a_2\theta_2 + a_3\theta_3, \\ a_0 + a_4\theta_4 + a_5\theta_5 &= a_6\theta_6 + b_1\theta_3. \end{aligned} \tag{15}$$

Rearranging Eq. (15) to solve for θ_2 and θ_5 in terms of S and θ_3 results in

$$a_2\theta_2 = S + C_1 - a_3\theta_3, \qquad a_5\theta_5 = C_2 + b_1\theta_3 \tag{16}$$

where

$$C_1 = a_6\theta_6 - a_1\theta_1, \qquad C_2 = a_6\theta_6 - a_4\theta_4 - a_0. \tag{17}$$

Solving the inverse kinematics of linkage at zero cyclic pitch angle results in

$$\Theta_1 = \Theta_4 = \frac{\pi}{2}. \tag{18}$$

Substituting Eq. (18) into (17) results in

$$C_1 = a_6\theta_6 - a_1 i, \qquad C_2 = a_6\theta_6 - a_4 i - a_0. \tag{19}$$

Equation (19) is used to eliminate θ_2 and θ_5 in Eq. (16). Multiplying both sides of the Eq. (16) by their complex conjugate parts and using the unit vector relations $\theta_2\bar{\theta}_2 = 1$ and $\theta_5\bar{\theta}_5 = 1$, where bar denotes the complex conjugate, results in

$$\begin{aligned} &a_2^2 = (S + C_1 - a_3\theta_3)\left(\bar{S} + \bar{C}_1 - a_3\theta_3^{-1}\right), \qquad a_5^2 = (C_2 + b_1\theta_3)\left(\bar{C}_2 + b_1\theta_3^{-1}\right), \\ &S = \bar{S}. \end{aligned} \tag{20}$$

Expanding Eq. (20) results in

$$\begin{aligned} &f_j = \alpha_{0j} + \alpha_{1j}\theta_3 + \alpha_{2j}S + \beta_{1j}\theta_3^{-1} + \beta_{2j}\theta_3^{-1}S = 0, \quad j = 1, 2, \\ &f_3 = \bar{S} - S = 0 \end{aligned} \tag{21}$$

where

$$\begin{aligned} &\alpha_{01} = C_1\bar{S} + C_1\bar{C}_1 + a_3^2 - a_2^2, \qquad \alpha_{02} = b_1^2 - a_5^2 + C_2\bar{C}_2, \\ &\alpha_{11} = -a_3(\bar{C}_1 + \bar{S}), \qquad \alpha_{12} = b_1\bar{C}_2, \\ &\alpha_{21} = \bar{S} + \bar{C}_1, \qquad \alpha_{22} = 0, \\ &\beta_{11} = -C_1 a_3, \qquad \beta_{12} = b_1 C_2, \\ &\beta_{21} = -a_3, \qquad \beta_{22} = 0. \end{aligned} \tag{22}$$

The result of multiplying each of the three equations in Eq. (21) by the monomials 1, θ_3, and S and using the Sylvester-Type Elimination method [15] is

$$\mathbf{Q}_{9\times 9}\mathbf{m}_{9\times 1} = 0 \tag{23}$$

where $\mathbf{m}_{9\times 1}$ is the vector of the monomials and $\mathbf{Q}_{9\times 9}$ is the matrix obtained by multiplying Eq. (21) by the monomials as

$$\mathbf{Q}_{9\times 9} = \begin{bmatrix} \alpha_{01} & \alpha_{11} & \alpha_{21} & 0 & 0 & 0 & \beta_{11} & \beta_{21} & 0 \\ \beta_{11} & \alpha_{01} & \beta_{21} & \alpha_{11} & \alpha_{21} & 0 & 0 & 0 & 0 \\ 0 & 0 & \alpha_{01} & 0 & \alpha_{11} & \alpha_{21} & 0 & \beta_{11} & \beta_{21} \\ \alpha_{02} & \alpha_{12} & \alpha_{22} & 0 & 0 & 0 & \beta_{12} & \beta_{22} & 0 \\ \beta_{12} & \alpha_{02} & \beta_{22} & \alpha_{12} & \alpha_{22} & 0 & 0 & 0 & 0 \\ 0 & 0 & \alpha_{02} & 0 & \alpha_{12} & \alpha_{22} & 0 & \beta_{12} & \beta_{22} \\ \bar{S} & 0 & -1 & 0 & 0 & 0 & 0 & 0 & 0 \\ 0 & \bar{S} & 0 & 0 & -1 & 0 & 0 & 0 & 0 \\ 0 & 0 & \bar{S} & 0 & 0 & -1 & 0 & 0 & 0 \end{bmatrix}, \qquad \mathbf{m}_{9\times 1} = \begin{bmatrix} 1 \\ \theta_3 \\ S \\ \theta_3^2 \\ \theta_3 S \\ S^2 \\ \theta_3^{-1} \\ \theta_3^{-1}S \\ \theta_3^{-1}S^2 \end{bmatrix}. \tag{24}$$

Factoring the variable $\bar{S}$ from Eq. (24) and splitting the matrix $\mathbf{Q}$ into the sparse matrices $\mathbf{Q}_1$ and $\mathbf{Q}_2$ results in

$$(\mathbf{Q}_1 + \mathbf{Q}_2\bar{S})\mathbf{m} = 0 \tag{25}$$

where

$$\mathbf{Q}_{1_{9\times 9}} = \begin{bmatrix} \gamma_1 & \gamma_2 & \gamma_3 & 0 & 0 & 0 & \beta_{11} & \beta_{21} & 0 \\ \beta_{11} & \gamma_1 & \beta_{21} & \gamma_2 & \gamma_3 & 0 & 0 & 0 & 0 \\ 0 & 0 & \gamma_1 & 0 & \gamma_2 & \gamma_3 & 0 & \beta_{11} & \beta_{21} \\ \alpha_{02} & \alpha_{12} & \alpha_{22} & 0 & 0 & 0 & \beta_{12} & \beta_{22} & 0 \\ \beta_{12} & \alpha_{02} & \beta_{22} & \alpha_{12} & \alpha_{22} & 0 & 0 & 0 & 0 \\ 0 & 0 & \alpha_{02} & 0 & \alpha_{12} & \alpha_{22} & 0 & \beta_{12} & \beta_{22} \\ 0 & 0 & -1 & 0 & 0 & 0 & 0 & 0 & 0 \\ 0 & 0 & 0 & 0 & -1 & 0 & 0 & 0 & 0 \\ 0 & 0 & 0 & 0 & 0 & -1 & 0 & 0 & 0 \end{bmatrix}, \tag{26}$$

$$\mathbf{Q}_{2_{9\times 9}} = \begin{bmatrix} C_1 & -a_3 & 1 & 0 & 0 & 0 & 0 & 0 & 0 \\ 0 & C_1 & 0 & -a_3 & 1 & 0 & 0 & 0 & 0 \\ 0 & 0 & C_1 & 0 & -a_3 & 1 & 0 & 0 & 0 \\ 0 & 0 & 0 & 0 & 0 & 0 & 0 & 0 & 0 \\ 0 & 0 & 0 & 0 & 0 & 0 & 0 & 0 & 0 \\ 0 & 0 & 0 & 0 & 0 & 0 & 0 & 0 & 0 \\ 1 & 0 & 0 & 0 & 0 & 0 & 0 & 0 & 0 \\ 0 & 1 & 0 & 0 & 0 & 0 & 0 & 0 & 0 \\ 0 & 0 & 1 & 0 & 0 & 0 & 0 & 0 & 0 \end{bmatrix}, \tag{27}$$

and $\gamma_1 = C_1\bar{C}_1 + a_3^2 - a_2^2$, $\gamma_2 = -a_3\bar{C}_1$ and $\gamma_3 = \bar{C}_1$. In order for Eq. (25) to have a non-trivial solution, the following condition must hold:

$$\mathbf{Q}_1\mathbf{m} = -\bar{S}\mathbf{Q}_2\mathbf{m}. \tag{28}$$

Equation (28) is a generalized eigenvalue problem and can be solved by the QZ decomposition method [18]. Also, this equation can be easily solved in MATLAB using this command:

$$S = \text{eig}\big(\mathbf{Q}_1, \mathbf{Q}_2, \text{'}qz\text{'}\big). \tag{29}$$

Given the collective pitch angle, δ_{col}, the vertical displacement of the swashplate z_c is calculated as

$$z_c = h_{e_6} - S \tag{30}$$

where h_{e_6} is the fixed height of the rotor grip from the point O, shown in Fig. 2 and its value is listed in Table 2.

The above method provides a fast numerical solution for the nonlinear kinematics of the Bell–Hiller mixer. Since the matrices $\mathbf{Q}_1$ and $\mathbf{Q}_2$ in Eqs. (26) and (27) are square matrices of dimension 9, solving the inverse kinematics of the Bell–Hiller mixer using the above method results in 9 solutions. This is a significant reduction compared to [9] with 48 solutions. The true solution of the inverse kinematics is obtained by applying physical constraints of the mechanism. The range of z_c is [4.5 9.5] cm, so, solutions for z_c that are complex or out of range are ignored.

2.4 Cyclic pitch to swashplate orientations

Given the swashplate vertical displacement z_c in Eq. (30), the inverse kinematic equations of the Bell–Hiller mixer are derived so that the orientations of the swashplate expressed by

the Euler angles δ_x and δ_y are obtained in terms of the lateral and longitudinal cyclic pitch angles δ_{lat} and δ_{lon}. First, a local coordinates $\{x_1 y_1 z_1\}$ attached to the swashplate's moving upper plate at the point C is defined as shown in Fig. 2. Then, according to Eq. (12), the kinematic equations are derived once at the azimuth angle $\Psi = 0°$, to solve for δ_y in terms of the longitudinal cyclic pitch δ_{lon}, and once at the azimuth angle $\Psi = 90°$, to solve for δ_x in terms of the lateral cyclic pitch δ_{lat}.

A similar procedure is followed to derive the kinematic equations for the orientation of the swashplate. Since the tilting angles of the swashplate to the cyclic pitch angle are desired, here the variables S, θ_4 and θ_6 are defined as the inputs, and θ_1, θ_2, θ_3 and θ_5 are defined as the outputs of the mechanism. Rearranging Eq. (15) to solve for θ_2 and θ_5 in terms of θ_1 and θ_3 results in

$$a_2\theta_2 = C_3 - a_3\theta_3 - a_1\theta_1, \qquad a_5\theta_5 = C_2 + b_1\theta_3 \tag{31}$$

where

$$C_2 = a_6\theta_6 - a_0 - a_4\theta_4, \qquad C_3 = S + a_6\theta_6 \tag{32}$$

where S is obtained from Eq. (29). Since the stabilizer bar's effect as a secondary input to the cyclic pitch can be included in the flapping equations of the helicopter model used for control design, for example in [16], the flapping angle of the stabilizer bar is again considered zero ($\Theta_4 = \frac{\pi}{2}$), and Eq. (32) is rewritten as

$$C_2 = a_6\theta_6 - a_0 - a_4 i, \qquad C_3 = S + a_6\theta_6. \tag{33}$$

Equation (33) is used to eliminate θ_2 and θ_5 in Eq. (31). Multiplying both sides of Eq. (31) by their complex conjugate parts and using the unit vector relations $\theta_2\bar{\theta}_2 = 1$ and $\theta_5\bar{\theta}_5 = 1$ results in:

$$\begin{aligned} &a_2^2 = (C_3 - a_3\theta_3 - a_1\theta_1)\big(\bar{C}_3 - a_3\theta_3^{-1} - a_1\bar{\theta}_1\big), \qquad a_5^2 = (C_2 + b_1\theta_3)\big(\bar{C}_2 + b_1\theta_3^{-1}\big), \\ &\theta_1\bar{\theta}_1 = 1. \end{aligned} \tag{34}$$

Expanding Eq. (34) results in:

$$\begin{aligned} &f_j = \alpha'_{0j} + \alpha'_{1j}\theta_3 + \alpha'_{2j}\theta_1 + \beta'_{1j}\theta_3^{-1} + \beta'_{2j}\theta_3^{-1}\theta_1 = 0, \quad j = 1, 2, \\ &f_3 = \theta_1\bar{\theta}_1 - 1 = 0 \end{aligned} \tag{35}$$

where

$$\begin{aligned} &\alpha'_{01} = -a_1 C_3\bar{\theta}_1 + C_3\bar{C}_3 + a_3^2 - a_2^2, \qquad \alpha'_{02} = b_1^2 - a_5^2 + C_2\bar{C}_2, \\ &\alpha'_{11} = -a_3(\bar{C}_3 - a_1\bar{\theta}_1), \qquad \alpha'_{12} = b_1\bar{C}_2, \\ &\alpha'_{21} = a_1^2\bar{\theta}_1 - a_1\bar{C}_3, \qquad \alpha'_{22} = 0, \\ &\beta'_{11} = -a_3 C_3, \qquad \beta'_{12} = b_1 C_2, \\ &\beta'_{21} = a_1 a_3, \qquad \beta'_{22} = 0. \end{aligned} \tag{36}$$

Multiplying each of the three equations in Eq. (35) by the monomials 1, θ_1 and θ_3, and applying the Sylvester-Type Elimination method results in

$$\mathbf{Q}'_{9\times 9}\mathbf{m}'_{9\times 1} = 0 \tag{37}$$

where $\mathbf{m}'_{9\times1}$ is the vector of the monomials and $\mathbf{Q}'_{9\times9}$ is the matrix obtained by multiplying Eq. (35) by the monomials as

$$\mathbf{Q}'_{9\times9}=\begin{bmatrix}\alpha'_{01} & \alpha'_{11} & \alpha'_{21} & 0 & 0 & 0 & \beta'_{11} & \beta'_{21} & 0\\ \beta'_{11} & \alpha'_{01} & \beta'_{21} & \alpha'_{11} & \alpha'_{21} & 0 & 0 & 0 & 0\\ 0 & 0 & \alpha'_{01} & 0 & \alpha'_{11} & \alpha'_{21} & 0 & \beta'_{11} & \beta'_{21}\\ \alpha'_{02} & \alpha'_{12} & \alpha'_{22} & 0 & 0 & 0 & \beta'_{12} & \beta'_{22} & 0\\ \beta'_{12} & \alpha'_{02} & \beta'_{22} & \alpha'_{12} & \alpha'_{22} & 0 & 0 & 0 & 0\\ 0 & 0 & \alpha'_{02} & 0 & \alpha'_{12} & \alpha'_{22} & 0 & \beta'_{12} & \beta'_{22}\\ -1 & 0 & \bar{\theta}_1 & 0 & 0 & 0 & 0 & 0 & 0\\ 0 & -1 & 0 & 0 & \bar{\theta}_1 & 0 & 0 & 0 & 0\\ 0 & 0 & -1 & 0 & 0 & \bar{\theta}_1 & 0 & 0 & 0\end{bmatrix},\qquad \mathbf{m}'_{9\times1}=\begin{bmatrix}1\\ \theta_3\\ \theta_1\\ \theta_3^2\\ \theta_3\theta_1\\ \theta_1^2\\ \theta_3^{-1}\\ \theta_3^{-1}\theta_1\\ \theta_3^{-1}\theta_1^2\end{bmatrix}. \tag{38}$$

Factoring the variable $\bar{\theta}_1$ from Eq. (38) and splitting the matrix $\mathbf{Q}'$ into the sparse matrices $\mathbf{Q}'_1$ and $\mathbf{Q}'_2$ results in

$$\left(\mathbf{Q}'_1+\mathbf{Q}'_2\bar{\theta}_1\right)\mathbf{m}'=0 \tag{39}$$

where

$$\mathbf{Q}'_{1_{9\times9}}=\begin{bmatrix}\gamma'_1 & \gamma'_2 & \gamma'_3 & 0 & 0 & 0 & \beta'_{11} & \beta'_{21} & 0\\ \beta'_{11} & \gamma'_1 & \beta'_{21} & \gamma'_2 & \gamma'_3 & 0 & 0 & 0 & 0\\ 0 & 0 & \gamma'_1 & 0 & \gamma'_2 & \gamma'_3 & 0 & \beta'_{11} & \beta'_{21}\\ \alpha'_{02} & \alpha'_{12} & \alpha'_{22} & 0 & 0 & 0 & \beta'_{12} & \beta'_{22} & 0\\ \beta'_{12} & \alpha'_{02} & \beta'_{22} & \alpha'_{12} & \alpha'_{22} & 0 & 0 & 0 & 0\\ 0 & 0 & \alpha'_{02} & 0 & \alpha'_{12} & \alpha'_{22} & 0 & \beta'_{12} & \beta'_{22}\\ -1 & 0 & 0 & 0 & 0 & 0 & 0 & 0 & 0\\ 0 & -1 & 0 & 0 & 0 & 0 & 0 & 0 & 0\\ 0 & 0 & -1 & 0 & 0 & 0 & 0 & 0 & 0\end{bmatrix}, \tag{40}$$

$$\mathbf{Q}'_{2_{9\times9}}=\begin{bmatrix}-a_1C_3 & a_1a_3 & a_1^2 & 0 & 0 & 0 & 0 & 0 & 0\\ 0 & -a_1C_3 & 0 & a_1a_3 & a_1^2 & 0 & 0 & 0 & 0\\ 0 & 0 & -a_1C_3 & 0 & a_1a_3 & a_1^2 & 0 & 0 & 0\\ 0 & 0 & 0 & 0 & 0 & 0 & 0 & 0 & 0\\ 0 & 0 & 0 & 0 & 0 & 0 & 0 & 0 & 0\\ 0 & 0 & 0 & 0 & 0 & 0 & 0 & 0 & 0\\ 0 & 0 & 1 & 0 & 0 & 0 & 0 & 0 & 0\\ 0 & 0 & 0 & 0 & 1 & 0 & 0 & 0 & 0\\ 0 & 0 & 0 & 0 & 0 & 1 & 0 & 0 & 0\end{bmatrix}, \tag{41}$$

and $\gamma'_1=C_3\bar{C}_3+a_3^2-a_2^2$, $\gamma'_2=-a_3\bar{C}_3$ and $\gamma'_3=-a_1\bar{C}_3$.

Therefore, given the longitudinal and lateral cyclic inputs δ_{lon} and δ_{lat} and the vertical displacement of the swashplate z_c, the tilt angle of the swashplate Θ_1 is

$$\Theta_1=\arg(\bar{\theta}_1) \tag{42}$$

where $\bar{\theta}_1$ is a complex number calculated using the QZ decomposition method as

$$\bar{\theta}_1=\text{eig}\left(\mathbf{Q}'_1,\mathbf{Q}'_2,\text{'}qz\text{'}\right). \tag{43}$$

The true solution of the inverse kinematics from Eqs. (42) and (43) is obtained by applying physical constraints of the mechanism. The range of Θ_1 is $[-15^\circ\ 15^\circ]$, so solutions for Θ_1 that are complex or out of range are ignored.

A linear approximation of the inverse kinematics of the Bell–Hiller mixer is derived using the small-angle assumptions to compare with the nonlinear model and is:

$$\begin{aligned}\delta_{\text{col}} &= \frac{\ell_{e_7e_8}}{\ell_{e_3e_7}\ell_{e_6e_8}}(z_c - z_0),\\ \delta_{\text{lon}} &= -\frac{\ell_{e_7e_8}r_1}{\ell_{e_3e_7}\ell_{e_6e_8}}(\Theta_{1_{\text{lon}}}),\\ \delta_{\text{lat}} &= \frac{\ell_{e_7e_8}r_1}{\ell_{e_3e_7}\ell_{e_6e_8}}(\Theta_{1_{\text{lat}}}),\end{aligned} \tag{44}$$

where z_0 is the height of the swashplate from the point O shown in Fig. 2, at zero collective pitch. The parameters of the linear approximation of the Bell–Hiller mixer kinematics in Eq. (44) are listed in Table 2. The dimensions of the actuating mechanisms are measured using a FARO arm machine.

Note that the longitudinal and lateral tilt angle of the swashplate, $\Theta_{1_{\text{lon}}}$ and $\Theta_{1_{\text{lat}}}$, are calculated in Eq. (42), which are not necessarily equal to the swashplate's Euler angles δ_x and δ_y. To obtain the Euler angles of the swashplate in general, two basis vectors are defined as

$$\hat{\boldsymbol{n}}_1 = \mathbf{R}_{y,\Theta_{1_{\text{lon}}}}[1 \quad 0 \quad 0 \quad 0]^T, \qquad \hat{\boldsymbol{n}}_2 = \mathbf{R}_{x,\Theta_{1_{\text{lat}}}}[0 \quad 1 \quad 0 \quad 0]^T \tag{45}$$

where $\hat{\boldsymbol{n}}_1$ and $\hat{\boldsymbol{n}}_2$ are the perpendicular unity vectors on the tilted plane of the swashplate and $\mathbf{R}$ is the rotation matrix defined in Eq. (3).

Defining $\hat{\boldsymbol{n}}_3$ as the normal vector of the tilted plane of the swashplate, it is calculated as

$$\hat{\boldsymbol{n}}_3 = \hat{\boldsymbol{n}}_1 \times \hat{\boldsymbol{n}}_2. \tag{46}$$

The normal vector $\hat{\boldsymbol{n}}_3$ could also be derived in terms of the tilt angles of the swashplate δ_x and δ_y using the homogeneous transformation $\mathbf{H}_1^i$ defined in Eq. (2) as

$$\hat{\boldsymbol{n}}_3 = \mathbf{H}_1^i[0 \quad 0 \quad 1 \quad 0]^T = [n_{31} \quad n_{32} \quad n_{33} \quad 0]^T. \tag{47}$$

Equating Eqs. (46) and (47) results in the swashplate's Euler angles as

$$\delta_x = -\arcsin(n_{32}), \qquad \delta_y = \arcsin\left(\frac{n_{31}}{\cos\delta_x}\right). \tag{48}$$

Combining Eqs. (10), (29) and (42) results in the inverse kinematics of the entire main rotor actuating mechanism representing the four swash servo inputs θ_{11} to θ_{41} in terms of the collective pitch angle δ_{col} and longitudinal and lateral cyclic pitch angles of the main rotor δ_{lon} and δ_{lat}. This is essential for the control implementation for small-scale helicopters as described in [16, 17]. There, a model-based nonlinear controller using the Sliding Mode Control (SMC) algorithm is designed to calculate the required collective and cyclic pitch angles, and then the above inverse kinematic solution for the swashplate and Bell–Hiller mixer is used to calculate the corresponding swash servo angles required for the desired maneuver. The forward and inverse kinematics of the tail rotor are described in the next section.

3 Tail rotor mechanism

The tail rotor has a complex mechanism composed of two planar linkage mechanisms shown in Fig. 3. The four-bar linkage mechanism "1234", moves the L-shape link "345" pivoted at

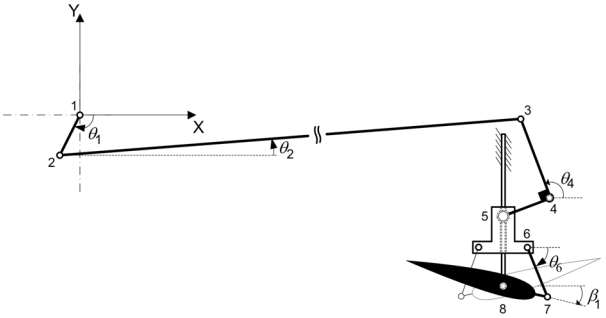

Fig. 3 Helicopter tail mechanism

point "4". An spherical joint at point "5", connects this link to a T-shape link which slides on the spinning shaft of the tail rotor. As the T-bar slides on the shaft, the pitch angle of the tail blade changes through another linkage mechanism "5678".

To derive the forward kinematics of the tail rotor mechanism, two kinematic loops "12341" and "56785" are defined and the kinematic equations are derived by writing the loop-closure equations for each loop. Writing the kinematic equations for the loop-closure "12341" results in

$$\boldsymbol{l}_{12} + \boldsymbol{l}_{23} = \boldsymbol{l}_{14} + \boldsymbol{l}_{43}. \tag{49}$$

Expanding (49) in the Cartesian coordinates results in

$$c_1 \cos\theta_1 + c_2 \cos\theta_2 = c_4 \cos\theta_4 + x_4, \qquad c_1 \sin\theta_1 + c_2 \sin\theta_2 = c_4 \sin\theta_4 + y_4 \tag{50}$$

where $c_1 = |\boldsymbol{l}_{12}|$, $c_2 = |\boldsymbol{l}_{23}|$, $c_4 = |\boldsymbol{l}_{43}|$, and x_4 and y_4 are the horizontal and vertical distance of the point "4" form the origin of the X–Y coordinates, respectively.

Rearranging Eq. (50) results in

$$c_2 \cos\theta_2 = m_1 + c_4 \cos\theta_4, \qquad c_2 \sin\theta_2 = m_2 + c_4 \sin\theta_4 \tag{51}$$

where $m_1 = x_4 - c_1 \cos\theta_1$ and $m_2 = y_4 - c_1 \sin\theta_1$. Adding the squares of the equations in Eq. (51) and eliminating θ_2 results in

$$c_2^2 = (m_1 + c_4 \cos\theta_4)^2 + (m_2 + c_4 \sin\theta_4)^2. \tag{52}$$

Solving Eq. (52) for θ_4 results in

$$\theta_4 = \arccos\left(\frac{c_2^2 - c_4^2 - m_1^2 - m_2^2}{2c_4 m_1} \cos\gamma_1\right) + \gamma_1 \tag{53}$$

where $\gamma_1 = \arctan(\frac{m_2}{m_1})$. Equation (53) provides a nonlinear relation between the angle of the L-shape link, θ_4, and the servo input θ_1.

Writing the kinematic equations for the loop-closure "56785" results in

$$\boldsymbol{l}_{15} + \boldsymbol{l}_{56} + \boldsymbol{l}_{67} = \boldsymbol{l}_{18} + \boldsymbol{l}_{87}. \tag{54}$$

Expanding Eq. (54) in the Cartesian coordinates results in

$$x_{56} + c_6 \cos\theta_6 = c_8 \cos\beta_1, \qquad y_5 + y_{56} + c_6 \sin\theta_6 = y_8 + c_8 \sin\beta_1 \tag{55}$$

where $c_6 = |\boldsymbol{l}_{67}|$, $c_8 = |\boldsymbol{l}_{87}|$, and x_{56} and y_{56} are the fixed horizontal and vertical offsets between the points "5" and "6" on the T-shaped link and y_8 is the fixed vertical offset of the

point "8" from the origin of the X–Y coordinates. The variable y_5 is the vertical displacement of the slider from the origin of the X–Y coordinates and is calculated as

$$y_5 = y_4 + b_4 \cos\theta_4 \tag{56}$$

where $b_4 = |\boldsymbol{l}_{45}|$. Substituting Eq. (56) into Eq. (55) results in

$$c_6 \cos\theta_6 = m_3 + c_8 \cos\beta_1, \qquad c_6 \sin\theta_6 = m_4 + c_8 \sin\beta_1 \tag{57}$$

where $m_3 = -x_{56}$ and $m_4 = y_8 - y_5 - y_{56}$. Adding the squares of the equations in Eq. (57) and eliminating θ_6 results in

$$c_6^2 = (m_3 + c_8 \cos\beta_1)^2 + (m_4 + c_8 \sin\beta_1)^2. \tag{58}$$

Solving Eq. (58) for β_1 yields

$$\beta_1 = \arcsin\left(\frac{c_6^2 - c_8^2 - m_3^2 - m_4^2}{2c_8 m_4} \cos\gamma_2\right) - \gamma_2 \tag{59}$$

where $\gamma_2 = \arctan(\frac{m_3}{m_4})$. Equation (59) provides a nonlinear relation between the pitch angle of the tail blade, β_1, and the angle of the L-shape link, θ_1. Therefore, combining Eqs. (53) and (59) results in the forward kinematics of the tail mechanism allowing the calculation of the pitch angle of the tail blade β_1, in terms of the tail servo input θ_1. The second tail blade is actuated through a mirrored mechanism as shown in Fig. 3 and its pitch angle is equal and opposite to that of the first blade.

The inverse kinematics of the tail mechanism is required to calculate the desired servo inputs for the control design. The inverse kinematics can be obtained by following a similar procedure on the same kinematic loops "12341" and "56785". Rearranging and solving Eq. (57) for θ_4 in terms of β_1, and then solving Eq. (51) for θ_1 in terms of θ_4 results in the inverse kinematics of the tail mechanism as

$$\theta_1 = \arccos\left(\frac{(m_1')^2 + (m_2')^2 + c_1^2 - c_2^2}{2c_1 m_1'} \cos\gamma_1'\right) + \gamma_1' \tag{60}$$

where

$$\begin{aligned}
m_1' &= c_4 \cos\theta_4 + x_4, & \theta_4 &= \arccos\left(\frac{m_4' - c_6 \sin\theta_6}{b_4}\right),\\
m_2' &= c_4 \sin\theta_4 + y_4, & \theta_6 &= \arccos\left(\frac{m_3'}{c_6}\right),\\
m_3' &= c_8 \cos\beta_1 - x_{56}, & \gamma_1' &= \arctan\left(\frac{m_2'}{m_1'}\right),\\
m_4' &= y_8 + c_8 \sin\beta_1 - y_{56} - y_4.
\end{aligned}$$

Again, a linear approximation of the inverse kinematics of the tail mechanism is derived for the comparison with the nonlinear model using a small-angle assumption as

$$\delta_{\text{ped}} = \frac{c_1 b_4}{c_4 c_8}\left(\theta_{\text{tail}} + \frac{\pi}{2}\right) + \delta_{0_{\text{tail}}} \tag{61}$$

where

$$\delta_{\text{ped}} = \beta_1, \qquad \theta_{\text{tail}} = \theta_1 - \frac{\pi}{2} \tag{62}$$

Table 2 Parameters of the main rotor actuating mechanism (values are in mm)

$x_{p1} = 18.6$	$y_{p1} = 1.8$	$\ell_{11} = 17.5$	$\ell_{31} = 14$	$r_1 = 23$	$\ell_{e_7e_8} = 25$
$x_{p2} = -19.4$	$y_{p2} = 48.2$	$\ell_{12} = 72.6$	$\ell_{32} = 74$	$r = 39.2$	$\ell_{e_3e_7} = 38$
$x_{p3} = -19.4$	$y_{p3} = 1.8$	$\ell_{21} = 18$	$\ell_{41} = 18$	$z_0 = 69$	$\ell_{e_6e_8} = 30.6$
$x_{p4} = 18.6$	$y_{p4} = -48.2$	$\ell_{22} = 72.9$	$\ell_{42} = 73.5$	$h_{e_6} = 168$	

Table 3 Parameters of the tail rotor actuating mechanism (values are in mm)

$c_1 = 17.53$	$c_4 = 31.87$	$c_6 = 10.5$	$x_4 = 1018$	$x_{56} = 11.32$	$y_8 = -86.7$
$c_2 = 1019$	$b_4 = 15.14$	$c_8 = 14.8$	$y_4 = -60$	$y_{56} = -15.43$	

and $\theta_{0_{\text{tail}}} = 0.1169$ rad is the pitch angle of the tail blade when $\theta_{\text{tail}} = 0$. The parameter of the linear approximation of the tail rotor mechanism are listed in Table 3. In addition, the tail rotor pitch can be expressed in terms of the pulse width of the tail servo as

$$\theta_{\text{tail}} = \alpha_{\text{tail}}(PW) + \delta_{0_{\text{tail}}} \tag{63}$$

where PW is the pulse width of the pulse width modulation (PWM) servo signal in seconds and the coefficients $\alpha_{\text{tail}} = -1698.5$ rad/s and $\delta_{0_{\text{tail}}} = 1.4724$ rad are obtained from the calibration diagram of the tail servo.

4 Experimental validation of the kinematic model

To validate the inverse kinematic models of the main rotor represented by Eqs. (10), (29) and (42) and the tail rotor kinematic model in Eq. (60), a 2000 pulse per revolution (PPR) optical encoder is attached to each blade grip of the main rotor and one blade grip of the tail rotor on the helicopter.

The data collection process is automated. The servo signals and the measurement data from the encoders are collected at the same time using a PCI-6602 National Instrument data acquisition card and a PC running the xPC Target real-time kernel. The experiments consist of commanding PWM signals to the servos of the helicopter and measuring the corresponding blade pitch angles using the optical encoders. For example, to validate the inverse kinematic model of the collective pitch to the swashplate displacement in Eq. (30), the stabilizer bar is fixed at zero flapping angle and the four servos of the main rotor are commanded such that the swashplate moves vertically and z_c increases from 60 to 80 mm in increments of about 2.5 mm. This is shown in Fig. 4, while the tilt of the swashplate is kept at zero ($\delta_x = \delta_y = 0$), and at the same time, the corresponding encoder measurements from each blade grip are collected. The data collected, as shown in Fig. 4, is limited to collective pitch angles between $-12°$ and $15°$ used in a normal flight maneuver.

The above process is repeated for the longitudinal and lateral cyclic tests and the tail rotor mechanism. The experimental data and the predicted responses of the nonlinear kinematics of the helicopter's actuating mechanisms are compared in Figs. 4, 5, 6 and 7, and shows a good match between the predicted nonlinear kinematic model of the main and tail rotor mechanisms and the experimental data. The inverse kinematics of the actuating mechanisms of the helicopter are thus experimentally validated.

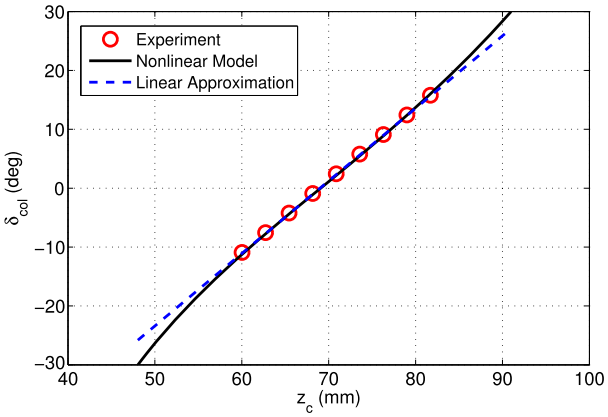

Fig. 4 Experimental results of the collective pitch of the main rotor versus vertical displacement of the swashplate and comparison to the nonlinear model and linear approximation. The measurement accuracy is ±0.3°

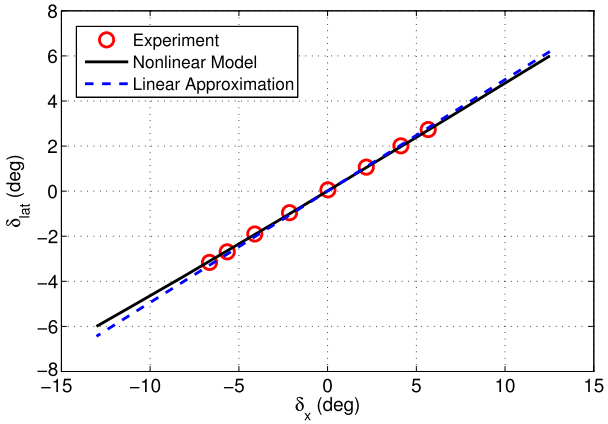

Fig. 5 Experimental results of the lateral cyclic pitch versus swashplate orientation and comparison to the nonlinear model and linear approximation. The measurement accuracy is ±0.5°

4.1 Experimental comparison of the nonlinear and linear kinematic models

The predicted response of the nonlinear model and the linear approximations of the kinematics of the helicopter's actuating mechanisms are also compared and shown by error bars in Figs. 4–7. The results indicate that the Bell–Hiller mixer and the tail rotor mechanism of the helicopter are designed such that the kinematic models obtained from the linear approximations accurately represent the nonlinear and actual kinematics of the system within a limited range of the servo angles required for normal maneuvers but deviate for a larger range of servo angles. For example, in the collective pitch of the main rotor versus swashplate vertical displacement graph shown in Fig. 4, the linear approximation model deviates 4.2° from the prediction of the nonlinear kinematic model at a collective pitch angle of −30°.

5 Conclusions

A fast and efficient inverse kinematic solution has been developed for the main and tail rotor actuating mechanisms of small-scale unmanned helicopters by deriving a detailed nonlinear equation of the Bell–Hiller mechanism and converting it into a generalized eigenvalue problem which is suitable for real-time control design of these vehicles. Also, a closed-form

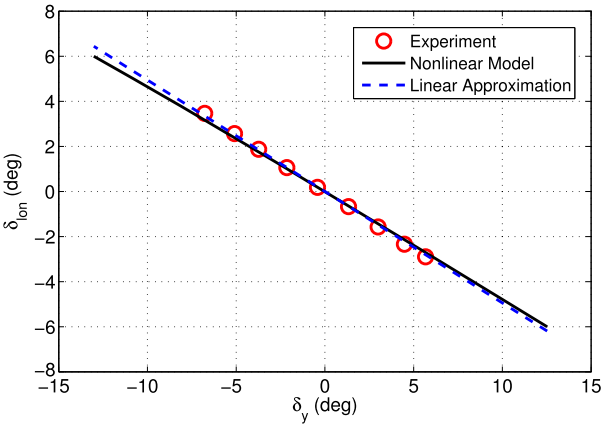

Fig. 6 Experimental results of the longitudinal cyclic pitch versus swashplate orientation and comparison to the nonlinear model and linear approximation. The measurement accuracy is ±0.5°

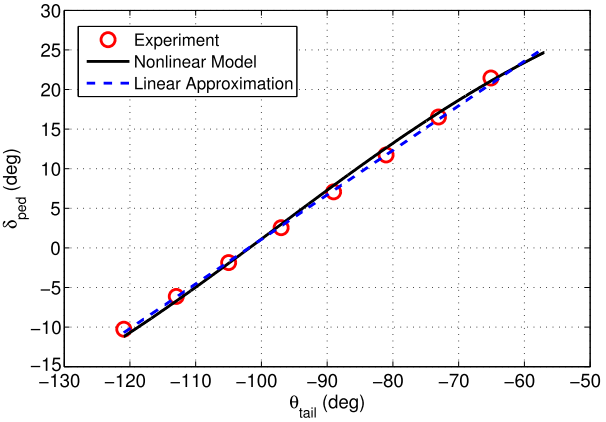

Fig. 7 Experimental results of the tail blade pitch versus tail servo arm input and comparison to the nonlinear model and linear approximation. The measurement accuracy is ±0.3°

inverse kinematic solution has been developed for a four-point swashplate mechanism which requires less torques from the servos. The linear approximation of the nonlinear kinematic model is also derived. The kinematic models of the main and tail rotor mechanisms have been validated by the careful correlation of the model with experimental results. The results demonstrate a good match between the predicted nonlinear kinematic model and the experimental data. Moreover, this methodology is applicable to similar mechanisms with no change and the developed nonlinear model can be used by designers to find the exact linear operation range of their designed Bell–Hiller mixer and tail rotor mechanism.

References

1. Battezzato, A., Sorli, A., Pastorelli, S.: Kinematic and dynamic modeling of a helicopter rigid main rotor. In: ASME International Design Engineering Technical Conferences and Computers and Information in Engineering Conference, Brooklyn, NY, pp. 435–442 (2008)
2. Kim, S.K., Tilbury, D.M.: Mathematical modeling and experimental identification of an unmanned helicopter robot with flybar dynamics. J. Robot. Syst. **21**(3), 95–116 (2004)
3. Cai, G., Chen, B.M., Lee, T.H., Lum, K.-Y.: Comprehensive nonlinear modeling of a miniature unmanned helicopter. J. Am. Helicopter Soc. **57**(1), 1–13 (2012)

4. Mettler, B., Tischler, M.B., Kanade, T.: System identification modeling of a small-scale unmanned rotorcraft for flight control design. J. Am. Helicopter Soc. **47**(1), 50–63 (2002)
5. Mettler, B., Dever, C., Feron, E.: Scaling effects and dynamic characteristics of miniature rotorcraft. J. Guid. Control Dyn. **27**(3), 466–478 (2004)
6. Bristeau, P.J., Dorveaux, E., Vissiere, D., Petit, N.: Hardware and software architecture for state estimation on an experimental low-cost small-scaled helicopter. Control Eng. Pract. **18**, 733–746 (2010)
7. Lau, T.K., Liu, Y.H., Lin, K.W.: A New method of modeling the actuating dynamics of a miniature hingeless helicopter using gyroscopic moments. In: International Conference on Robotics and Automation (ICRA), Anchorage, AK, pp. 608–613 (2010)
8. Bortoff, S.A.: The University of Toronto RC helicopter: A test bed for nonlinear control. In: International Conference on Control Applications, Kohala, HI, pp. 333–338 (1999)
9. Sabaapour, M.R., Zohoor, H.: Analysis of a swashplate mechanism of the hingeless rotor hub with the flybar in a model helicopter, Part I: Kinematics. J. Syst. Des. Dyn. **4**(4), 616–631 (2010)
10. Lange, C., Ranjbaran, F., Angeles, J., Goritschnig, G.: The kinematics of the swashplate mechanism of a VTOL unmanned aerial vehicle. Multibody Syst. Dyn. **3**(4), 333–365 (1999)
11. Saffarian, M., Fahimi, F.: A comprehensive kinematic analysis of a model helicopter's actuating mechanism. In: 46th AIAA Aerospace Sciences Meeting and Exhibit, Reno, NV, pp. 1–15 (2008)
12. Tsai, L.W.: Robot Analysis: The Mechanics of Serial and Parallel Manipulators. Wiley, New York (1999)
13. Merlet, J.P.: An algorithm for the forward kinematics of general parallel manipulators. In: Fifth International Conference on Advanced Robotics, Pisa, Italy, pp. 1131–1135 (1991)
14. Angeles, J.: Fundamentals of Robotic Mechanical Systems: Theory, Methods, and Algorithms. Springer, New York (1997)
15. Wampler, C.W.: Solving the kinematics of planar mechanisms. J. Mech. Des. **121**(3), 387–391 (1999)
16. Khaligh, S.P.: Control-oriented modeling and system identification for nonlinear trajectory tracking control of a small-scale unmanned helicopter. Ph.D. Thesis, University of Alberta, Edmonton, Alberta (2014)
17. Khaligh, S.P., Martinez, A., Fahimi, F., Koch, C.R.: A HIL testbed for initial controller gain tuning of a small unmanned helicopter. J. Intell. Robot. Syst. **73**(1–4), 289–308 (2014)
18. Horn, R.: Matrix Analysis. Cambridge University Press, Cambridge, pp. 1–100 (1985)